molecules

MDPI

Article

Amino-Functionalized Titanium Based Metal-Organic Framework for Photocatalytic Hydrogen Production

Niannian Hu [1], Youlie Cai [1], Lan Li [2], Xusheng Wang [1,3,4,*] and Junkuo Gao [1,3,*]

[1] Institute of Functional Porous Materials, School of Materials Science and Engineering, Zhejiang Sci-Tech University, Hangzhou 310018, China; 202030302117@mails.zstu.edu.cn (N.H.); 201920301012@mails.zstu.edu.cn (Y.C.)
[2] College of Materials Science and Engineering, China Jiliang University, Hangzhou 310018, China; lilan123@mail.ustc.edu.cn
[3] Zhejiang Provincial Innovation Center of Advanced Textile Technology, Shaoxing 312000, China
[4] College of Chemistry and Materials Science, Jinan University, Guangzhou 510632, China
* Correspondence: xswang@zstu.edu.cn (X.W.); jkgao@zstu.edu.cn (J.G.)

Abstract: Photocatalytic hydrogen production using stable metal-organic frameworks (MOFs), especially the titanium-based MOFs (Ti-MOFs) as photocatalysts is one of the most promising solutions to solve the energy crisis. However, due to the high reactivity and harsh synthetic conditions, only a limited number of Ti-MOFs have been reported so far. Herein, we synthesized a new amino-functionalized Ti-MOFs, named NH_2-ZSTU-2 (ZSTU stands for Zhejiang Sci-Tech University), for photocatalytic hydrogen production under visible light irradiation. The NH_2-ZSTU-2 was synthesized by a facile solvothermal method, composed of 2,4,6-tri(4-carboxyphenylphenyl)-aniline (NH_2-BTB) triangular linker and infinite Ti-oxo chains. The structure and photoelectrochemical properties of NH_2-ZSTU-2 were fully studied by powder X-ray diffraction, scanning electron microscope, nitro sorption isotherms, solid-state diffuse reflectance absorption spectra, and Mott–Schottky measurements, etc., which conclude that NH_2-ZSTU-2 was favorable for photocatalytic hydrogen production. Benefitting from those structural features, NH_2-ZSTU-2 showed steady hydrogen production rate under visible light irradiation with average photocatalytic H_2 yields of 431.45 $\mu mol \cdot g^{-1} \cdot h^{-1}$ with triethanolamine and Pt as sacrificial agent and cocatalyst, respectively, which is almost 2.5 times higher than that of its counterpart ZSTU-2. The stability and proposed photocatalysis mechanism were also discussed. This work paves the way to design Ti-MOFs for photocatalysis.

Keywords: metal-organic frameworks; photocatalytic hydrogen production; amino-functionalized; titanium; photocatalyst

check for updates

Citation: Hu, N.; Cai, Y.; Li, L.; Wang, X.; Gao, J. Amino-Functionalized Titanium Based Metal-Organic Framework for Photocatalytic Hydrogen Production. *Molecules* **2022**, *27*, 4241. https://doi.org/10.3390/molecules27134241

Academic Editor: Tifeng Xia

Received: 9 June 2022
Accepted: 29 June 2022
Published: 30 June 2022

1. Introduction

Photocatalytic hydrogen production from water using solar light as clean and sustainable energy is one of the most promising solutions to solve the energy crisis [1–5]. As a new kind of porous materials, metal-organic frameworks (MOFs) have been applied in many fields such as gas adsorption/storage/separation, sensor, drug delivery, batteries, electrocatalysis, photocatalysis, due to their ultrahigh surface area and void space, adjustable structure, tunable pore sizes, and modifiable internal surfaces [6–21]. Since Mori et al. first reported that MOFs can achieve photocatalytic hydrogen production, a series of MOFs have been reported to show potential in this application [22–29]. However, most of those MOFs survived low stability during photocatalysis process.

Titanium-based MOFs (Ti-MOFs), as a kind of robust MOFs, are constructed by organic ligands and high valent Ti^{4+} ions, showing high chemical stability [9,30]. The high stability of Ti-MOFs can be explained by the Pearson's hard-soft acid-base principle, in which carboxylate ligands can be seen as hard base, and the high valent Ti^{4+} ions as hard acid, thus, robust coordination bond between carboxylate ligand and Ti^{4+} ions are

formed [7]. Moreover, titanium ions are preferred to form Ti-oxo clusters or infinite Ti-oxo chains/sheets, which will be coordinated with many ligands, further strengthening the stability of Ti-MOFs. However, due to the high reactivity and harsh synthetic conditions of titanium precursors, only a limited number of Ti-MOFs have been reported so far [31–45].

Among the various semiconductors, TiO_2 is the first example used for photocatalytic hydrogen production due to its light sensitive Ti ions [46]. Superior to TiO_2, Ti-MOFs not only possess Ti-oxo clusters or Ti-oxo chains/sheets, but also have light harvested ligands, endowing them with promising photocatalytic activity [47]. Especially, the adjustable structures of Ti-MOFs make them efficiently utilize the solar light beyond ultraviolet region (accounts only 4%). Herein, we synthesized an amino functionalized Ti-MOF, named NH_2-ZSTU-2 (ZSTU stands for Zhejiang Sci-Tech University), for photocatalytic hydrogen production. This MOF is composed of infinite Ti-oxo chains and amino functionalized ternary carboxylic acid ligands, which is isomorphic to ZSTU-2 (Figure 1). Compared with the counterpart ZSTU-2, NH_2-ZSTU-2 showed a nearly 2.5 times higher photocatalytic hydrogen production activity with a rate of 431.45 $\mu mol \cdot g^{-1} \cdot h^{-1}$.

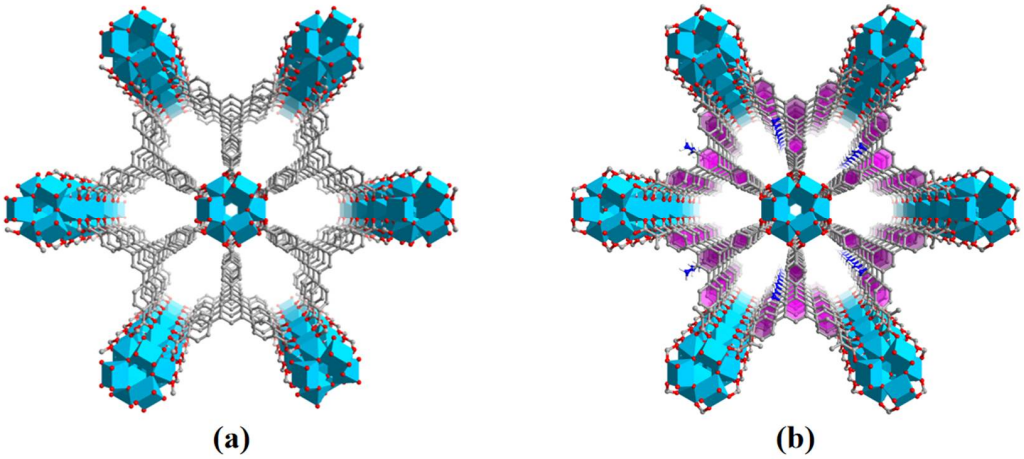

Figure 1. Crystal structures of the ZSTU-2 (**a**) and NH_2-ZSTU-2 (**b**).

2. Results and Discussions

2.1. Structural Characterizations of Photocatalysts

The crystallinity of NH_2-ZSTU-2 was improved by introducing acetic acid as the modulator, which can delay the crystallization speed of MOF, and finally obtain better crystallinity. The regular rod-shaped crystallites with diameter of approximately 50 nm and length of 150 nm were characterized by scanning electron microscope (SEM), which is isomorphic to ZSTU-2 (Figure 2). The size of NH_2-ZSTU-2 is too small to directly determine the crystal structure using single-crystal diffraction measurements. Therefore, powder X-ray diffraction (PXRD) analysis was used to discovery the MOF structure. The PXRD pattern of NH_2-ZSTU-2 is quite similar to ZSTU-2 (Figure S1), and we thus modeled the structure of NH_2-ZSTU-2 using the framework of ZSTU-2 with installed amino group on BTB linkers, followed by structural optimization using material studio. Based on the structure model, Pawley refinement was performed on the PXRD data, and we obtained the unit cell parameters of a = 11. 7987 Å, b = 34.6036 Å, and c = 20.1266 Å, and $\alpha = \beta = \gamma = 90°$, with agreement factors of $R_p = 0.0720$ and $R_{wp} = 0.0943$ for NH_2-ZSTU-2 (Figure 3), strongly supporting its validity. Detailed lattice parameters and atomic coordinates of NH_2-ZSTU-2 are provided in Tables S1 and S2. Based on the structure of NH_2-ZSTU-2 we obtained by Pawley refinement, every six titanium atoms form a secondary unit of $Ti_6(\mu_3\text{-}O)_6(COO)_6$ through a bridge, while such a Ti_6 cluster is interconnected on the c-axis by adjacent μ_2-OH to form an infinite one-dimensional $[Ti_6(\mu_3\text{-}O)_6(\mu_3\text{-}OH)_6(COO)_6]_n$ chain of titanium-oxygen clusters. The 1D Ti-oxo chains were then extended by the triangular NH_2-BTB linkers to form a 3D porous structure. The high porous structure of NH_2-ZSTU-2 was further studied

by nitrogen sorption isotherms (Figure 4). The calculated BET specific surface area from nitrogen sorption isotherms is about 604 m^2/g, which is comparable to its counterparts ZSTU-2 (657 m^2/g). Through the infrared (IR) spectrogram (Figure S2), we can find that the titanium oxide bonds had been formed in both NH_2-ZSTU-2 and ZSTU-2, with the corresponding vibration band near 773 cm^{-1} [38]. Furthermore, IR vibration band at approximately 1430 cm^{-1}, 1604 cm^{-1}, 3459 cm^{-1} are associated with the C-O stretching vibration, the benzene ring skeleton vibration, and the stretching vibration of hydroxyl coordination, respectively. Compared with ZSTU-2, an extra vibration band near 3399 cm^{-1} of NH_2-ZSTU-2 can be attributed to the uncoordinated amino group. In addition, we found that the IR peak at 3399 cm^{-1} was kept but 3459 cm^{-1} was decreased after heating the NH_2-ZSTU-2 at 200 °C for 2 h under vacuum, which indicated that the absorbed water was vapored and the amino groups were retained after heating. In order to obtain the thermal stability of the MOFs, thermogravimetry analysis (TG) was further studied (Figure S3). Through the TG curves, we can conclude that both NH_2-ZSTU-2 and ZSTU-2 can maintain their structure at about 400 °C. The weight loss at around 200 °C is mainly attributed to the loss of coordinated solvents in MOFs.

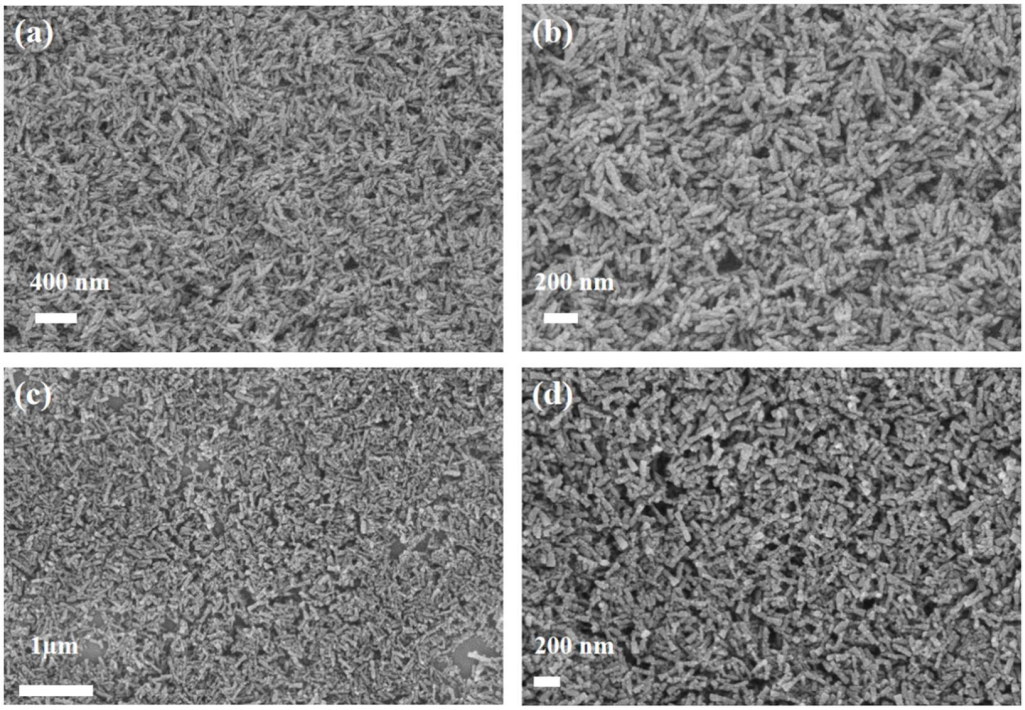

Figure 2. SEM images of ZSTU-2 (**a**,**b**) and NH_2-ZSTU-2 (**c**,**d**).

As we know, the band structures determine thermodynamics of photocatalysts for photocatalytic hydrogen production. The band gaps of ZSTU-2 and NH_2-ZSTU-2 were first studied by solid-state diffuse reflectance absorption spectra. As shown in Figure 5a, the light harvesting region of ZSTU-2 can only reach 450 nm, and the corresponding band gap calculated from Tauc plot is 3.29 eV (Figure 5b). To extend the absorption range of ZSTU-2 to visible region, amino functionalized NH_2-BTB linkers were adopted to replace the H_3BTB linkers during MOF synthesis. The light absorption region of the NH_2-ZSTU-2 illustrated by solid-state diffuse reflectance absorption spectra can be largely extended to 700 nm (Figure 5c), and the band gap is only 2.24 eV (Figure 5d). For photocatalysts, the larger light-harvesting region and lower band gap mean that they can utilize more sunlight and achieve better photocatalytic hydrogen production performance. The conduction band positions of ZSTU-2 and NH_2-ZSTU-2 were further determined by Mott–Schottky measurements. Positive slope in both Figure 5e,f indicated that both ZSTU-2 and NH_2-ZSTU-2 are n-type semiconductors. The conduction band potentials of them were determined to be −0.68 eV

and −0.66 eV, respectively. Then the valence band potentials of them were calculated to be 2.61 eV and 1.58 eV, respectively. The energy band diagram of ZSTU-2 and NH_2-ZSTU-2 are shown in Figure S4. The introduction of amino groups in MOFs mainly shifts the valence band potential to a higher position and shows little impact on the conduction band potential. Based on the band structural information, we can conclude that both ZSTU-2 and NH_2-ZSTU-2 were favorable for photocatalytic hydrogen production.

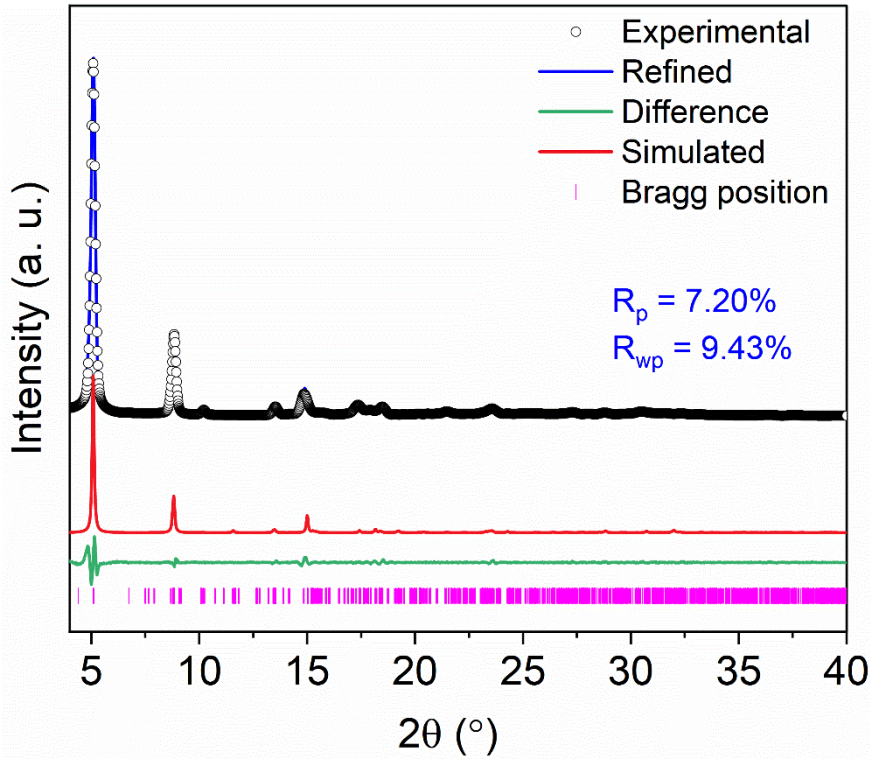

Figure 3. The PXRD analysis of NH_2-ZSTU-2 displaying the experimental pattern (black circles), refined pattern based on Pawley refinement (blue line), the difference plot (green line), the simulated plot (red line), and Bragg positions (pink).

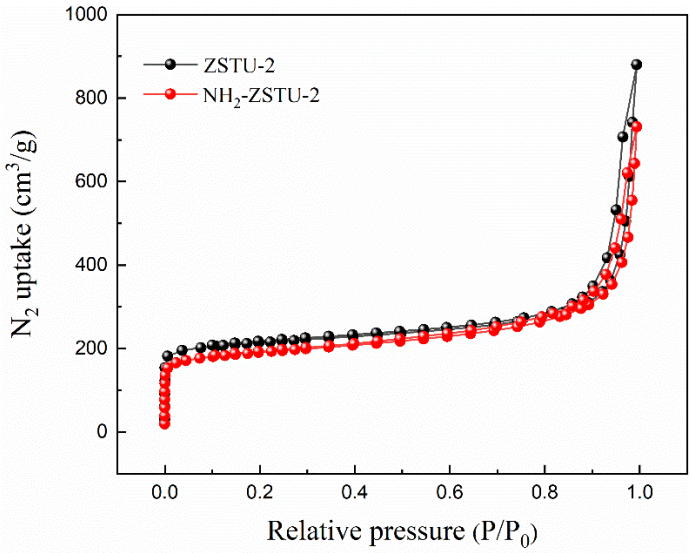

Figure 4. Nitrogen sorption isotherms of ZSTU-2 and NH_2-ZSTU-2.

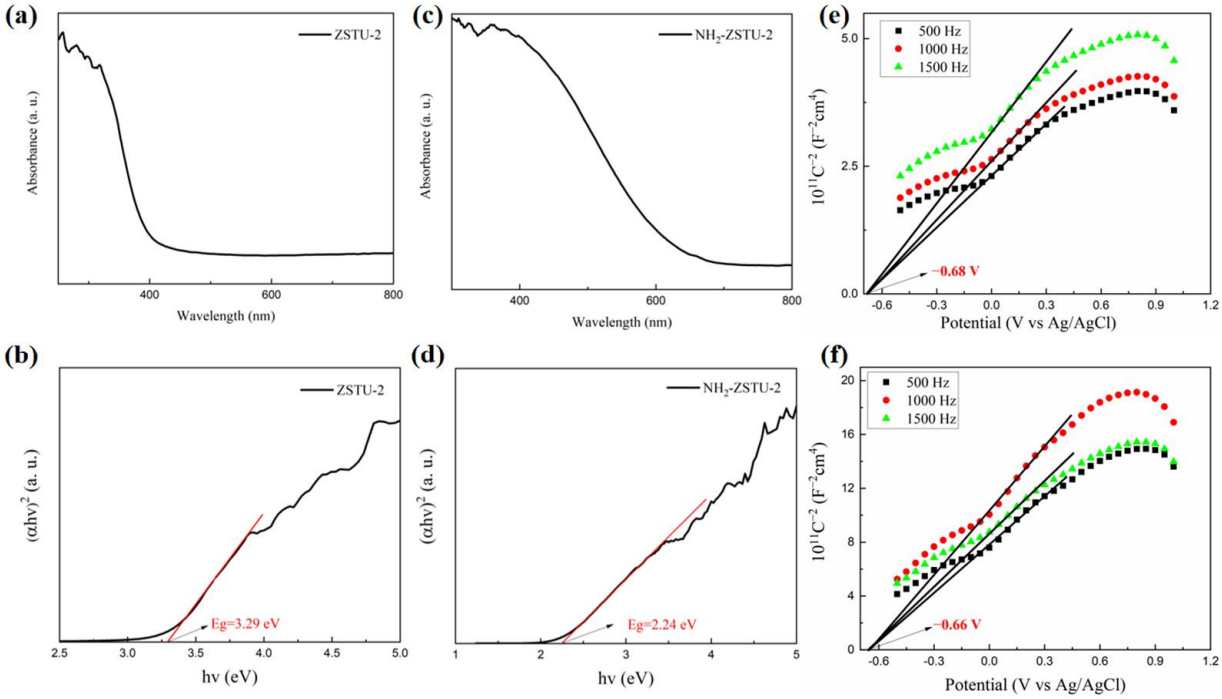

Figure 5. Band structural information of photocatalysts. The solid-state diffuse reflectance absorption spectra of ZSTU-2 (**a**) and NH_2-ZSTU-2 (**c**); Tauc plots for ZSTU-2 (**b**) and NH_2-ZSTU-2 (**d**), presenting band gap of MOFs calculated under the hypothesis that absorption follows: $(\alpha h\nu)^2 = K (h\nu - E_g)$; Mott–Schottky plots of ZSTU-2 (**e**) and NH_2-ZSTU-2 (**f**).

2.2. Photoelectrochemical Characterizations of Photocatalysts

The generation of separated electron-hole pairs was characterized by both transient photocurrent responses and electrochemical impedance spectroscopy (EIS) measurements. As shown in Figure 6a, ZSTU-2 showed low transient photocurrent response under visible light due to the narrow light-harvesting region. As expected, the transient photocurrent responses of NH_2-ZSTU-2 increased dramatically, which indicated that a better photogenerated charge carries separation efficiency. The EIS of NH_2-ZSTU-2 was further studied both with and without visible light irradiation. As shown in Figure 6b, compared with the dark state, dramatically decreased radius of the EIS curve under visible light irradiation indicated that a large number of separated electron-hole pairs were photogenerated in NH_2-ZSTU-2 with visible light shining on.

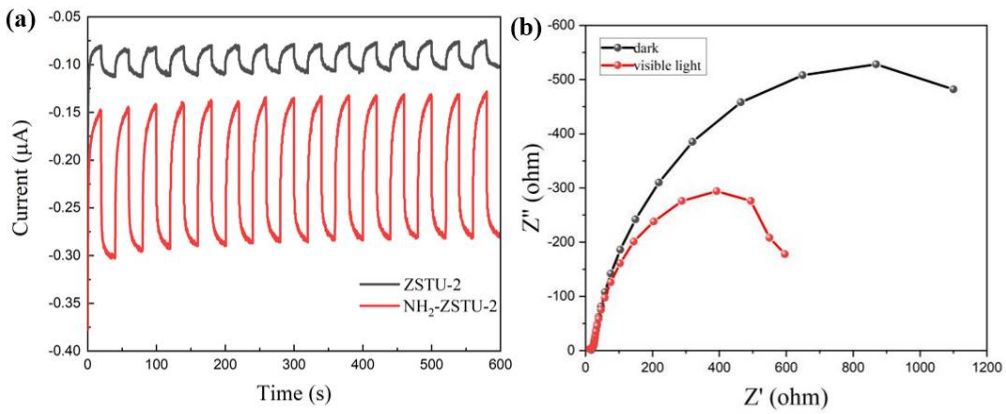

Figure 6. Photoelectrochemical characterizations of photocatalysts. Transient photocurrent plots of NH_2-ZSTU-2 and ZSTU-2 (**a**); EIS curves of NH_2-ZSTU-2 under dark and visible light (**b**).

2.3. Photocatalytic Hydrogen Production of Photocatalysts

Before photocatalytic hydrogen production, both MOFs were loaded with Pt using a photo deposition method [48]. The Pt nanoparticles were successfully deposited in MOFs and characterized by TEM (Figure S5). The photocatalytic hydrogen production was then performed in TEOA/CH_3CN/H_2O mixed solvents under 300 W Xe lamp irradiation with a L42 light filter and triethanolamine (TEOA) as a sacrificial agent, and Pt as cocatalyst [48]. Before the photocatalytic reaction, the solution was degassed for 20 min to remove the dissolved O_2 in solvent. The production of hydrogen was detected by an on-line GC with a TCD detector. As shown in Figure 7a, both Pt@ZSTU-2 and Pt@NH_2-ZSTU-2 showed steady hydrogen production rate under visible light irradiation. The average photocatalytic H_2 yields of Pt@ZSTU-2 and Pt@NH_2-ZSTU-2 were 170.45 $\mu mol \cdot g^{-1} \cdot h^{-1}$ and 431.45 $\mu mol \cdot g^{-1} \cdot h^{-1}$, respectively. The almost 2.5 times enhanced photocatalytic hydrogen production rate of Pt@NH_2-ZSTU-2 is mainly attributed to the enlarged light-harvested region. It should be noted that the cocatalyst Pt plays important role on photocatalytic hydrogen production. The hydrogen production rate of Pt@NH_2-ZSTU-2 is also comparable to the state-of-the-art Ti-MOFs, such as PCN-416 (484 $\mu mol \cdot g^{-1} \cdot h^{-1}$), MIL-100(Ti) (42 $\mu mol \cdot g^{-1} \cdot h^{-1}$), MUV-10(Mn) (271 $\mu mol \cdot g^{-1} \cdot h^{-1}$), NH_2-MIL-125 (367 $\mu mol \cdot g^{-1} \cdot h^{-1}$) [28,49–51]. The stability of Pt@NH_2-ZSTU-2 during photocatalysis was studied by the recycle experiments, which indicated that Pt@NH_2-ZSTU-2 is stable at least three cycles under visible light irradiation. The hydrogen evolution rates of the first, second and third cycles were 431.45 $\mu mol \cdot g^{-1} \cdot h^{-1}$, 421.50 $\mu mol \cdot g^{-1} \cdot h^{-1}$ and 420.71 $\mu mol \cdot g^{-1} \cdot h^{-1}$, respectively (Figure 7b). The retained PXRD patterns of the recycled Pt@NH_2-ZSTU-2 also indicated that Pt@NH_2-ZSTU-2 is stable (Figure S3).

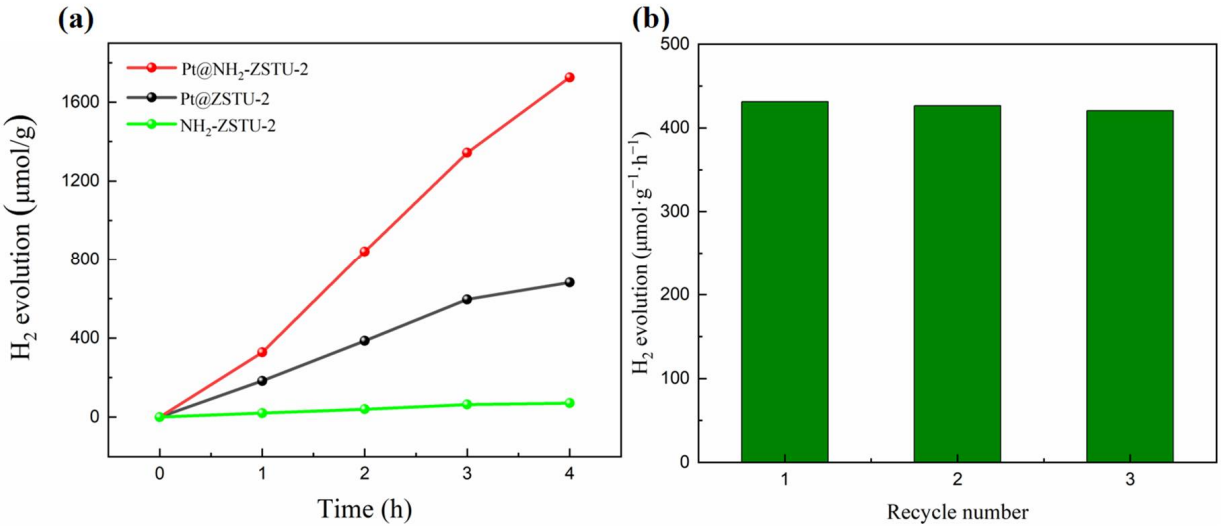

Figure 7. Photocatalytic performance. (**a**) Time-dependent photocatalytic hydrogen production of Pt@ZSTU-2, Pt@NH_2-ZSTU-2, and NH_2-ZSTU-2 in triethanolamine/acetonitrile/water system under visible light irradiation; (**b**) recycle performance of Pt@NH_2-ZSTU-2 under same condition.

A proposed, photocatalytic hydrogen evolution mechanism of Pt@NH_2-ZSTU-2 is shown in Figure 8. Under visible light irradiation, NH_2-BTB linkers absorb light and the generated photogenerated electrons then transfer to infinite Ti-oxo chains through LMCT mechanism, thus reducing Ti^{4+} to Ti^{3+}, and the photogenerated electrons in NH_2-ZSTU-2 conduction band transfer to Pt cocatalyst for reduction of water to produce H_2 [16,26,35]. The holes in the valence band oxidize the sacrificial agent TEOA to $TEOA^+$, constituting a complete REDOX reaction.

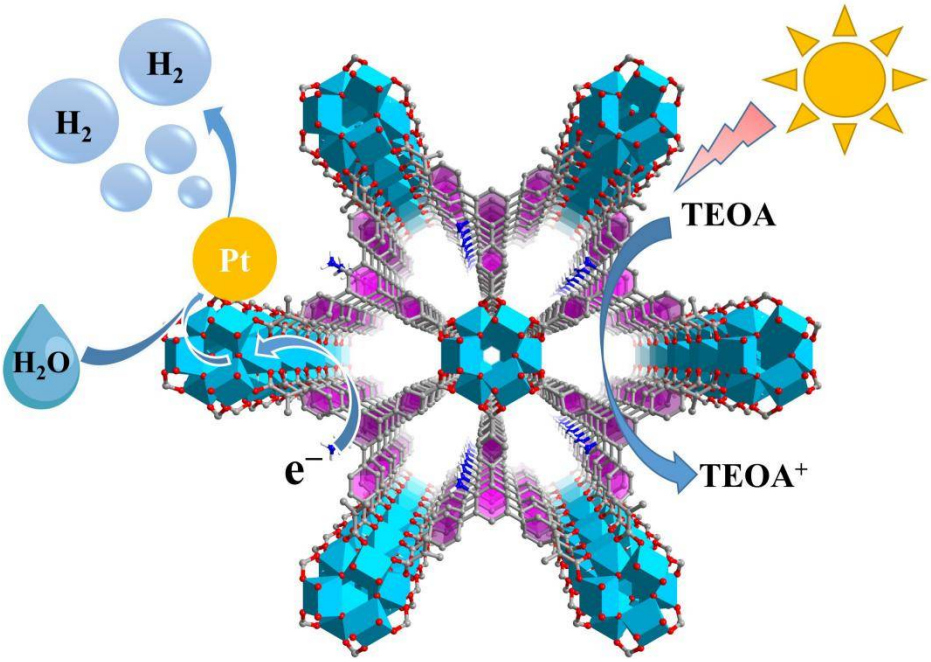

Figure 8. Proposed photocatalytic hydrogen production mechanism over NH_2-ZSTU-2 under visible light irradiation.

3. Experimental

3.1. Synthesis of NH_2-ZSTU-2

2,4,6-tris(4-carboxyphenyl)-aniline (NH_2-BTB) (100 mg, 0.220 mmol) and ultra-dry DMF (5 mL) were first added into a 25 mL Teflon-lined stainless-steel autoclave, and then 100 μL glacial acetic acid was added dropwise. After sonication for 10 min, NH_2-BTB was fully dissolved to obtain a yellow transparent solution, and then titanium tetraisopropanolate (Ti(i-Pro)$_4$) (0.04 mL, 0.128 mmol) was added dropwise, and sonication was performed for 20 min to form a yellow slurry. The autoclave was then heated in an oven at 190 °C for 22 h. After cooling down, the yellow powder NH_2-ZSTU-2 was obtained by centrifuging and washing with DMF and methanol for several times. At last, NH_2-ZSTU-2 was dried in a vacuum oven at 60 °C for 12 h to remove the residual methanol. CHN element analysis data of NH_2-ZSTU-2 had also been done with average weight ratio of 43.915:2.612:2.18. The chemical formula of NH_2-ZSTU-2 was determined to be $Ti_6(\mu_3\text{-}O)_6(\mu_2\text{-}OH)_6(NH_2\text{-}BTB)_2\ (DMF)_{0.3}$ based on element analysis and its structural information obtained from Pawley refinement of PXRD data.

3.2. Synthesis of Pt@NH_2-ZSTU-2

Pt NPs were deposited in the NH_2-ZSTU-2 using a photo deposition method [52]. First, NH_2-ZSTU-2 (50 mg) was dispersed in a mixture of H_2O (8 mL) and MeOH (13 mL) in a reaction vessel. After NH_2-ZSTU-2 was fully dispersed in the mixture, 1 mL chloroplatinic acid hexahydrate aqueous solution (1.33 mg·mL^{-1}) was then added and the system was vacuumed for 20 min to remove the air. The mixture was then irradiated with a 300 W Xe lamp without light filter for 4 h. The sample was then centrifuged and dried overnight in an oven at 100 °C, and resulted sample was labeled as Pt@NH_2-ZSTU-2. The chlorine and Pt content in NH_2-ZSTU-2 had been determined to be 1.25 wt% and 9.33 wt% by energy dispersive spectrometer (FESEM, JEOL, Japan).

3.3. Photoelectrochemical Measurementsz

Electrode Preparation: About 10 mg of photocatalyst was dispersed in 1 mL of isopropanol, and then 30 μL of naphthol solution (5% *w*/*w* in water) was added, and the mixture was sonicated for 2 h afterwards. The obtained dispersion was then dropped onto

one side of a FTO glass with an area of 1 × 1 cm^2 (total area of 1 × 3 cm^2), and dried in air at 60 °C on a hotplate.

Photocurrent measurements were carried out on an electrochemical workstation (Shanghai Chenhua Instrument Co. Ltd., Shanghai, China) in a standard three-electrode system with photocatalysts-coated FTO as the working electrode, Pt net as the counter electrode, Ag/AgCl as the reference electrode, and 0.5 M Na_2SO_4 solution (pH ≈ 7.0) as the electrolyte. A 300 W Xe lamp with a L42 light filter was used as visible light source, and the photo-responsive signals of photocatalysts was then recorded with alternating 20 s light on/off. Mott–Schottky plots of those photocatalysts were also performed on the same workstation in a standard three-electrode system at frequencies of 500, 1000, 1500 HZ. EIS curves were obtained using the same workstation and photocatalysts-coated FTO was used as the working electrode.

3.4. Photocatalytic Hydrogen Production Experiments

The photocatalytic hydrogen production experiments were evaluated using a batch-type reaction system (Beijing Perfectlight Technology, Beijing, China) at ambient temperature irradiated by a 300 W Xe lamp equipped with a UV cut-off filter (>420 nm). The temperature of condensed circulating water for cooling down the solvent vapor was set to 1 °C. In a typical procedure, 50 mg sample was dispersed into 102 mL mixed solution of acetonitrile, triethanolamine (TEOA), and de-ionized water with volume ratio of 9:1:0.2, and then the suspension was vacuumed for 10 min to remove air. Hydrogen gas was measured by an on-line gas chromatography (GC) (Techcomp-GC7900, argon as a carrier gas) using a thermal conductivity detector (TCD). The production of hydrogen was quantified by a calibration plot to the internal hydrogen standard. For the recycle experiment, the procedure is as follows: after the first experiment test, the system was vacuumed to remove the produced hydrogen and then the second run was restarted the next day. Same procedure was carried out for the third run. In this way, we can avoid the loss of photocatalyst during recovery.

4. Conclusions

In this work, we had synthesized an amino-functionalized Ti-MOF, named NH_2-ZSTU-2, for photocatalytic hydrogen production. The NH_2-ZSTU-2 was synthesized by a facile solvothermal method, composed of 2,4,6-tri(4-carboxyphenylphenyl)-aniline (NH_2-BTB) triangular linker and infinite Ti-oxo chains. The structure of NH_2-ZSTU-2 was fully studied by PXRD, SEM, nitrogen sorption isotherms, etc. The band structural information was also obtained by using solid-state diffuse reflectance absorption spectra and Mott-Schottky measurements, which conclude that NH_2-ZSTU-2 was favorable for photocatalytic hydrogen production. The generation of separated electron-hole pairs was also characterized by both transient photocurrent responses and electrochemical impedance spectroscopy (EIS) measurements, further showing the potential photocatalytic hydrogen production ability of NH_2-ZSTU-2. Benefitting from those structural features, NH_2-ZSTU-2 showed steady hydrogen production rate under visible light irradiation with average photocatalytic H_2 yields of 431.45 $\mu mol \cdot g^{-1} \cdot h^{-1}$ with triethanolamine and Pt as sacrificial agent and cocatalyst, respectively, which is almost 2.5 times higher than that of its counterpart ZSTU-2. The stability and proposed photocatalysis mechanism were also discussed. This work paves the way to design Ti-MOFs for photocatalysis.

Supplementary Materials: The following supporting information can be downloaded at: https://www.mdpi.com/article/10.3390/molecules27134241/s1, Figure S1: The PXRD patterns of the simulated ZSTU-2, as synthesized ZSTU-2, and NH2-ZSTU-2; Figure S2: Infrared spectra of the ZSTU-2, NH2-ZSTU-2, and NH2-ZSTU-2 after heating at 200 °C under vacuum; Figure S3: Thermogravimetry analysis of ZSTU-2 and NH_2-ZSTU-2 under nitrogen atmosphere; Figure S4: The energy band diagram of the ZSTU-2 and NH_2-ZSTU-2; Figure S5: TEM image of Pt@NH2-ZSTU-2; Figure S6: Powder XRD patterns of NH_2-ZSTU-2 before and after three cycles of photocatalytic hydrogen production; Table S1: Crystal data and refinement details; Table S2: Fractional atomic coordinates.

Author Contributions: Designed the experiments, X.W. and J.G.; conducted the experiments, N.H.; analyzed the data, N.H., Y.C., L.L. and X.W.; original draft, N.H.; review and editing, X.W. and J.G. All authors have read and agreed to the published version of the manuscript.

Funding: We are grateful for the financial support from the National Natural Science Foundation of China (Grant No. 22001094), Guangdong Basic and Applied Basic Research Foundation (Grant No. 2020A1515110003), and fundamental research funds of Zhejiang Sci-Tech University.

Institutional Review Board Statement: Not applicable.

Informed Consent Statement: Not applicable.

Data Availability Statement: Not applicable.

Conflicts of Interest: The authors declare no conflict of interest.

Sample Availability: Not applicable.

References

1. Zhang, X.; Tong, S.; Huang, D.; Liu, Z.; Shao, B.; Liang, Q.; Wu, T.; Pan, Y.; Huang, J.; Liu, Y.; et al. Recent advances of Zr based metal organic frameworks photocatalysis: Energy production and environmental remediation. *Coord. Chem. Rev.* **2021**, *448*, 214177. [CrossRef]
2. Sui, J.; Liu, H.; Hu, S.; Sun, K.; Wan, G.; Zhou, H.; Zheng, X.; Jiang, H.L. A General Strategy to Immobilize Single-Atom Catalysts in Metal-Organic Frameworks for Enhanced Photocatalysis. *Adv. Mater.* **2022**, *34*, 2109203. [CrossRef] [PubMed]
3. Wang, T.; Dai, Z.; Kang, J.; Fu, F.; Zhang, T.; Wang, S. A TiO_2 nanocomposite hydrogel for Hydroponic plants in efficient water improvement. *Mater. Chem. Phys.* **2018**, *215*, 242–250. [CrossRef]
4. Jiang, G.; Wang, R.; Wang, X.; Xi, X.; Hu, R.; Zhou, Y.; Wang, S.; Wang, T.; Chen, W. Novel highly active visible-light-induced photocatalysts based on BiOBr with Ti doping and Ag decorating. *ACS Appl. Mater. Interfaces* **2012**, *4*, 4440–4444. [CrossRef] [PubMed]
5. Wang, S.; Wang, T.; Ding, Y.; Su, Q.; Xu, Y.; Xu, Z.; Jiang, G.; Chen, W. Air-Water Interface Photocatalysis: A Realizable Approach for Decomposition of Aqueous Organic Pollutants. *Sci. Adv. Mater.* **2013**, *5*, 1006–1012. [CrossRef]
6. Melchionna, M.; Fornasiero, P. Updates on the Roadmap for Photocatalysis. *ACS Catal.* **2020**, *10*, 5493–5501. [CrossRef]
7. Wang, X.S.; Li, L.; Li, D.; Ye, J. Recent Progress on Exploring Stable Metal–Organic Frameworks for Photocatalytic Solar Fuel Production. *Sol. RRL* **2020**, *4*, 1900547. [CrossRef]
8. Liu, Y.; Huang, D.; Cheng, M.; Liu, Z.; Lai, C.; Zhang, C.; Zhou, C.; Xiong, W.; Qin, L.; Shao, B.; et al. Metal sulfide/MOF-based composites as visible-light-driven photocatalysts for enhanced hydrogen production from water splitting. *Coord. Chem. Rev.* **2020**, *409*, 213220. [CrossRef]
9. Li, L.; Wang, X.S.; Liu, T.F.; Ye, J. Titanium-Based MOF Materials: From Crystal Engineering to Photocatalysis. *Small Methods* **2020**, *4*, 2000486. [CrossRef]
10. Wang, X.; Yang, X.; Chen, C.; Li, H.; Huang, Y.; Cao, R. Graphene Quantum Dots Supported on Fe-based Metal-Organic Frameworks for Efficient Photocatalytic CO_2 Reduction. *Acta Chim. Sin.* **2022**, *80*, 22–28. [CrossRef]
11. Zhang, J.; Huang, J.; Wang, L.; Sun, P.; Wang, P.; Yao, Z.; Yang, Y. Coupling Bimetallic NiMn-MOF Nanosheets on $NiCo_2O_4$ Nanowire Arrays with Boosted Electrochemical Performance for Hybrid Supercapacitor. *Mater. Res. Bull.* **2022**, *149*, 111707. [CrossRef]
12. Li, G.; Cai, H.; Li, X.; Zhang, J.; Zhang, D.; Yang, Y.; Xiong, J. Construction of Hierarchical $NiCo_2O_4$@Ni-MOF Hybrid Arrays on Carbon Cloth as Superior Battery-Type Electrodes for Flexible Solid-State Hybrid Supercapacitors. *ACS Appl. Mater. Interfaces* **2019**, *11*, 37675–37684. [CrossRef]
13. Gao, J.; Cai, Y.; Qian, X.; Liu, P.; Wu, H.; Zhou, W.; Liu, D.X.; Li, L.; Lin, R.B.; Chen, B. A Microporous Hydrogen-Bonded Organic Framework for the Efficient Capture and Purification of Propylene. *Angew. Chem. Int. Ed.* **2021**, *60*, 20400–20406. [CrossRef] [PubMed]
14. Gao, J.; Qian, X.; Lin, R.B.; Krishna, R.; Wu, H.; Zhou, W.; Chen, B. Mixed Metal-Organic Framework with Multiple Binding Sites for Efficient C_2H_2 /CO_2 Separation. *Angew. Chem. Int. Ed.* **2020**, *59*, 4396–4400. [CrossRef] [PubMed]
15. Wang, X.-S.; Chen, C.-H.; Ichihara, F.; Oshikiri, M.; Liang, J.; Li, L.; Li, Y.; Song, H.; Wang, S.; Zhang, T.; et al. Integration of adsorption and photosensitivity capabilities into a cationic multivariate metal-organic framework for enhanced visible-light photoreduction reaction. *Appl. Catal. B Environ.* **2019**, *253*, 323–330. [CrossRef]
16. Huang, H.; Wang, X.-S.; Philo, D.; Ichihara, F.; Song, H.; Li, Y.; Li, D.; Qiu, T.; Wang, S.; Ye, J. Toward visible-light-assisted photocatalytic nitrogen fixation: A titanium metal organic framework with functionalized ligands. *Appl. Catal. B Environ.* **2020**, *267*, 118686. [CrossRef]
17. Luo, X.; Abazari, R.; Tahir, M.; Fan, W.K.; Kumar, A.; Kalhorizadeh, T.; Kirillov, A.M.; Amani-Ghadim, A.R.; Chen, J.; Zhou, Y. Trimetallic metal–organic frameworks and derived materials for environmental remediation and electrochemical energy storage and conversion. *Coord. Chem. Rev.* **2022**, *461*, 214505. [CrossRef]

18. Anwar, S.; Khan, F.; Zhang, Y.; Djire, A. Recent development in electrocatalysts for hydrogen production through water electrolysis. *Int. J. Hydrogen Energy* **2021**, *46*, 32284–32317. [CrossRef]
19. Zhou, Y.; Abazari, R.; Chen, J.; Tahir, M.; Kumar, A.; Ikreedeegh, R.R.; Rani, E.; Singh, H.; Kirillov, A.M. Bimetallic metal–organic frameworks and MOF-derived composites: Recent progress on electro- and photoelectrocatalytic applications. *Coord. Chem. Rev.* **2022**, *451*, 214264. [CrossRef]
20. Yan, Y.; Abazari, R.; Yao, J.; Gao, J. Recent strategies to improve the photoactivity of metal-organic frameworks. *Dalton Trans.* **2021**, *50*, 2342–2349. [CrossRef]
21. Gao, J.; Huang, Q.; Wu, Y.; Lan, Y.-Q.; Chen, B. Metal–Organic Frameworks for Photo/Electrocatalysis. *Adv. Energy Sustain. Res.* **2021**, *2*, 2100033. [CrossRef]
22. Kataoka, Y.; Sato, K.; Miyazaki, Y.; Masuda, K.; Tanaka, H.; Naito, S.; Mori, W. Photocatalytic hydrogen production from water using porous material $[Ru_2(p\text{-}BDC)_2]_n$. *Energy Environ. Sci.* **2009**, *2*, 397–400. [CrossRef]
23. Kong, X.J.; Lin, Z.; Zhang, Z.M.; Zhang, T.; Lin, W. Hierarchical Integration of Photosensitizing Metal-Organic Frameworks and Nickel-Containing Polyoxometalates for Efficient Visible-Light-Driven Hydrogen Evolution. *Angew. Chem. Int. Ed.* **2016**, *55*, 6411–6416. [CrossRef]
24. Han, S.Y.; Pan, D.L.; Chen, H.; Bu, X.B.; Gao, Y.X.; Gao, H.; Tian, Y.; Li, G.S.; Wang, G.; Cao, S.L.; et al. A Methylthio-Functionalized-MOF Photocatalyst with High Performance for Visible-Light-Driven H_2 Evolution. *Angew. Chem. Int. Ed.* **2018**, *57*, 9864–9869. [CrossRef] [PubMed]
25. Liu, H.; Xu, C.; Li, D.; Jiang, H.L. Photocatalytic Hydrogen Production Coupled with Selective Benzylamine Oxidation over MOF Composites. *Angew. Chem. Int. Ed.* **2018**, *57*, 5379–5383. [CrossRef]
26. Xiao, J.D.; Han, L.; Luo, J.; Yu, S.H.; Jiang, H.L. Integration of Plasmonic Effects and Schottky Junctions into Metal-Organic Framework Composites: Steering Charge Flow for Enhanced Visible-Light Photocatalysis. *Angew. Chem. Int. Ed.* **2018**, *57*, 1103–1107. [CrossRef]
27. Xiao, Y.; Qi, Y.; Wang, X.; Wang, X.; Zhang, F.; Li, C. Visible-Light-Responsive 2D Cadmium-Organic Framework Single Crystals with Dual Functions of Water Reduction and Oxidation. *Adv. Mater.* **2018**, *30*, 1803401. [CrossRef]
28. Yuan, S.; Qin, J.S.; Xu, H.Q.; Su, J.; Rossi, D.; Chen, Y.; Zhang, L.; Lollar, C.; Wang, Q.; Jiang, H.L.; et al. $[Ti_8Zr_2O_{12}(COO)_{16}]$ Cluster: An Ideal Inorganic Building Unit for Photoactive Metal-Organic Frameworks. *ACS Cent. Sci.* **2018**, *4*, 105–111. [CrossRef]
29. Kamakura, Y.; Chinapang, P.; Masaoka, S.; Saeki, A.; Ogasawara, K.; Nishitani, S.R.; Yoshikawa, H.; Katayama, T.; Tamai, N.; Sugimoto, K.; et al. Semiconductive Nature of Lead-Based Metal-Organic Frameworks with Three-Dimensionally Extended Sulfur Secondary Building Units. *J. Am. Chem. Soc.* **2020**, *142*, 27–32. [CrossRef]
30. Zhu, J.; Li, P.-Z.; Guo, W.; Zhao, Y.; Zou, R. Titanium-based metal–organic frameworks for photocatalytic applications. *Coord. Chem. Rev.* **2018**, *359*, 80–101. [CrossRef]
31. Yuan, S.; Feng, L.; Wang, K.; Pang, J.; Bosch, M.; Lollar, C.; Sun, Y.; Qin, J.; Yang, X.; Zhang, P.; et al. Stable Metal-Organic Frameworks: Design, Synthesis, and Applications. *Adv. Mater.* **2018**, *30*, 1704303. [CrossRef] [PubMed]
32. Serre, C.; Groves, J.A.; Lightfoot, P.; Slawin, A.M.Z.; Wright, P.A.; Stock, N.; Bein, T.; Haouas, M.; Taulelle, F.; Férey, G. Synthesis, Structure and Properties of Related Microporous N,N′-Piperazinebismethylenephosphonates of Aluminum and Titanium. *Chem. Mater.* **2006**, *18*, 1451–1457. [CrossRef]
33. Dan-Hardi, M.; Serre, C.; Frot, T.; Rozes, L.; Maurin, G.; Sanchez, C.; Ferey, G. A new photoactive crystalline highly porous titanium(IV) dicarboxylate. *J. Am. Chem. Soc.* **2009**, *131*, 10857–10859. [CrossRef] [PubMed]
34. Bueken, B.; Vermoortele, F.; Vanpoucke, D.E.P.; Reinsch, H.; Tsou, C.-C.; Valvekens, P.; De Baerdemaeker, T.; Ameloot, R.; Kirschhock, C.E.A.; Van Speybroeck, V.; et al. A Flexible Photoactive Titanium Metal-Organic Framework Based on a $[Ti(IV)_3(\mu_3\text{-}O)(O)_2(COO)_6]$ Cluster. *Angew. Chem. Int. Ed.* **2015**, *127*, 14118–14123. [CrossRef]
35. Keum, Y.; Park, S.; Chen, Y.P.; Park, J. Titanium-Carboxylate Metal-Organic Framework Based on an Unprecedented Ti-Oxo Chain Cluster. *Angew. Chem. Int. Ed.* **2018**, *57*, 14852–14856. [CrossRef] [PubMed]
36. Wang, S.; Kitao, T.; Guillou, N.; Wahiduzzaman, M.; Martineau-Corcos, C.; Nouar, F.; Tissot, A.; Binet, L.; Ramsahye, N.; Devautour-Vinot, S.; et al. A phase transformable ultrastable titanium-carboxylate framework for photoconduction. *Nat. Commun.* **2018**, *9*, 1660. [CrossRef]
37. Ziebel, M.E.; Darago, L.E.; Long, J.R. Control of Electronic Structure and Conductivity in Two-Dimensional Metal-Semiquinoid Frameworks of Titanium, Vanadium, and Chromium. *J. Am. Chem. Soc.* **2018**, *140*, 3040–3051. [CrossRef]
38. Li, C.; Xu, H.; Gao, J.; Du, W.; Shangguan, L.; Zhang, X.; Lin, R.-B.; Wu, H.; Zhou, W.; Liu, X.; et al. Tunable titanium metal–organic frameworks with infinite 1D Ti–O rods for efficient visible-light-driven photocatalytic H_2 evolution. *J. Mater. Chem. A* **2019**, *7*, 11928–11933. [CrossRef]
39. Padial, N.M.; Castells-Gil, J.; Almora-Barrios, N.; Romero-Angel, M.; da Silva, I.; Barawi, M.; Garcia-Sanchez, A.; de la Pena O'Shea, V.A.; Marti-Gastaldo, C. Hydroxamate Titanium-Organic Frameworks and the Effect of Siderophore-Type Linkers over Their Photocatalytic Activity. *J. Am. Chem. Soc.* **2019**, *141*, 13124–13133. [CrossRef]
40. Smolders, S.; Willhammar, T.; Krajnc, A.; Sentosun, K.; Wharmby, M.T.; Lomachenko, K.A.; Bals, S.; Mali, G.; Roeffaers, M.B.J.; De Vos, D.E.; et al. A Titanium(IV)-Based Metal-Organic Framework Featuring Defect-Rich Ti-O Sheets as an Oxidative Desulfurization Catalyst. *Angew. Chem. Int. Ed.* **2019**, *58*, 9160–9165. [CrossRef]

41. Cadiau, A.; Kolobov, N.; Srinivasan, S.; Goesten, M.G.; Haspel, H.; Bavykina, A.V.; Tchalala, M.R.; Maity, P.; Goryachev, A.; Poryvaev, A.S.; et al. A Titanium Metal-Organic Framework with Visible-Light-Responsive Photocatalytic Activity. *Angew. Chem. Int. Ed.* **2020**, *59*, 13468–13472. [CrossRef] [PubMed]
42. Keum, Y.; Kim, B.; Byun, A.; Park, J. Synthesis and Photocatalytic Properties of Titanium-Porphyrinic Aerogels. *Angew. Chem. Int. Ed.* **2020**, *59*, 21591–21596. [CrossRef] [PubMed]
43. Wang, S.; Cabrero-Antonino, M.; Navalón, S.; Cao, C.-c.; Tissot, A.; Dovgaliuk, I.; Marrot, J.; Martineau-Corcos, C.; Yu, L.; Wang, H.; et al. A Robust Titanium Isophthalate Metal-Organic Framework for Visible-Light Photocatalytic CO_2 Methanation. *Chem* **2020**, *6*, 3409–3427. [CrossRef]
44. Wang, S.; Reinsch, H.; Heymans, N.; Wahiduzzaman, M.; Martineau-Corcos, C.; De Weireld, G.; Maurin, G.; Serre, C. Toward a Rational Design of Titanium Metal-Organic Frameworks. *Matter* **2020**, *2*, 440–450. [CrossRef]
45. Zhu, Y.P.; Yin, J.; Abou-Hamad, E.; Liu, X.; Chen, W.; Yao, T.; Mohammed, O.F.; Alshareef, H.N. Highly Stable Phosphonate-Based MOFs with Engineered Bandgaps for Efficient Photocatalytic Hydrogen Production. *Adv. Mater.* **2020**, *32*, 1906368. [CrossRef]
46. Fujishima, A.; Honda, K. Electrochemical photolysis of water at a semiconductor electrode. *Nature* **1972**, *238*, 37–38. [CrossRef]
47. Yan, Y.; Li, C.; Wu, Y.; Gao, J.; Zhang, Q. From isolated Ti-oxo clusters to infinite Ti-oxo chains and sheets: Recent advances in photoactive Ti-based MOFs. *J. Mater. Chem. A* **2020**, *8*, 15245–15270. [CrossRef]
48. Kim, M.; Razzaq, A.; Kim, Y.K.; Kim, S.; In, S.-I. Synthesis and characterization of platinum modified TiO_2-embedded carbon nanofibers for solar hydrogen generation. *RSC Adv.* **2014**, *4*, 51286–51293. [CrossRef]
49. Castells-Gil, J.; Padial, N.M.; Almora-Barrios, N.; da Silva, I.; Mateo, D.; Albero, J.; García, H.; Martí-Gastaldo, C. De novo synthesis of mesoporous photoactive titanium(iv)–organic frameworks with MIL-100 topology. *Chem. Sci.* **2019**, *10*, 4313–4321. [CrossRef]
50. Castells-Gil, J.; Padial, N.M.; Almora-Barrios, N.; Albero, J.; Ruiz-Salvador, A.R.; Gonzalez-Platas, J.; Garcia, H.; Marti-Gastaldo, C. Chemical Engineering of Photoactivity in Heterometallic Titanium-Organic Frameworks by Metal Doping. *Angew. Chem. Int. Ed.* **2018**, *57*, 8453–8457. [CrossRef]
51. Horiuchi, Y.; Toyao, T.; Saito, M.; Mochizuki, K.; Iwata, M.; Higashimura, H.; Anpo, M.; Matsuoka, M. Visible-Light-Promoted Photocatalytic Hydrogen Production by Using an Amino-Functionalized Ti(IV) Metal–Organic Framework. *J. Phys. Chem. C* **2012**, *116*, 20848–20853. [CrossRef]
52. Remiro-Buenamañana, S.; Cabrero-Antonino, M.; Martínez-Guanter, M.; Álvaro, M.; Navalón, S.; García, H. Influence of co-catalysts on the photocatalytic activity of MIL-125(Ti)-NH_2 in the overall water splitting. *Appl. Catal. B Environ.* **2019**, *254*, 677–684. [CrossRef]